AGU100 ADVANCING EARTH AND SPACE SCIENCE

Geophysical Research Letters

RESEARCH LETTER
10.1029/2018GL079073

Special Section:
Curiosity at the Bagnold Dunes, Gale crater: Advances in Martian eolian processes

Sand Mineralogy Within the Bagnold Dunes, Gale Crater, as Observed In Situ and From Orbit

E. B. Rampe[1], M. G. A. Lapotre[2], T. F. Bristow[3], R. E. Arvidson[4], R. V. Morris[1], C. N. Achilles[5], C. Weitz[6], D. F. Blake[3], D. W. Ming[1], S. M. Morrison[7], D. T. Vaniman[6], S. J. Chipera[8], R. T. Downs[5], J. P. Grotzinger[9], R. M. Hazen[7], T. S. Peretyazhko[10], B. Sutter[10], V. Tu[10], A. S. Yen[11], B. Horgan[12], N. Castle[13], P. I. Craig[6], D. J. Des Marais[3], J. Farmer[14], R. Gellert[15], A. C. McAdam[16], J. M. Morookian[11], P. C. Sarrazin[17], and A. H. Treiman[13]

[1]Astromaterials Research and Exploration Science Division, NASA Johnson Space Center, Houston, TX, USA, [2]Department of Earth and Planetary Sciences, Harvard University, Cambridge, MA, USA, [3]NASA Ames Research Center, Moffett Field, CA, USA, [4]Department of Earth and Planetary Sciences, Washington University in St. Louis, St. Louis, MO, USA, [5]Department of Geosciences, University of Arizona, Tucson, AZ, USA, [6]Planetary Science Institute, Tucson, AZ, USA, [7]Geophysical Laboratory, Carnegie Institution for Science, Washington, DC, USA, [8]Chesapeake Energy, Oklahoma City, OK, USA, [9]Division of Geological and Planetary Sciences, California Institute of Technology, Pasadena, CA, USA, [10]Jacobs at NASA Johnson Space Center, Houston, TX, USA, [11]Jet Propulsion Laboratory, California Institute of Technology, Pasadena, CA, USA, [12]Department of Earth, Atmospheric, and Planetary Sciences, Purdue University, West Lafayette, IN, USA, [13]Lunar and Planetary Institute, Houston, TX, USA, [14]School of Earth and Space Exploration, Arizona State University, Tempe, AZ, USA, [15]Department of Physics, University of Guelph, Guelph, Ontario, Canada, [16]Goddard Space Flight Center, Greenbelt, MD, USA, [17]SETI Institute, Mountain View, CA, USA

Key Points:
- The mineralogy of active eolian sands were measured by the *Curiosity* rover at two locations in the Bagnold Dune Field in Gale crater, Mars
- X-ray diffraction data from the CheMin instrument of two sand samples indicate differences in plagioclase and olivine abundances
- The mineralogy derived from CheMin and CRISM can be used in concert to characterize sediment sorting and sources across the Bagnold Dunes

Supporting Information:
- Supporting Information S1
- Table S1

Correspondence to:
E. B. Rampe,
elizabeth.b.rampe@nasa.gov

Citation:
Rampe, E. B., Lapotre, M. G. A., Bristow, T. F., Arvidson, R. E., Morris, R. V., Achilles, C. N., et al. (2018). Sand mineralogy within the Bagnold Dunes, Gale crater, as observed in situ and from orbit. *Geophysical Research Letters, 45*, 9488–9497. https://doi.org/10.1029/2018GL079073

Received 7 JUN 2018
Accepted 23 AUG 2018
Accepted article online 29 AUG 2018
Published online 27 SEP 2018

Abstract *Curiosity* investigated active eolian sands near linear dunes during Phase 2 of the Bagnold Dunes campaign in Gale crater, Mars. Ogunquit Beach, a sample scooped from a large-ripple trough within the Mount Desert Island ripple field and delivered to the Chemistry and Mineralogy (CheMin) X-ray diffraction instrument, is dominated by basaltic igneous minerals and X-ray amorphous materials. CheMin mineralogy of the Gobabeb sample acquired at a large-ripple crest on the Namib barchan dune during Phase 1 is similar to Ogunquit Beach. Ogunquit Beach, however, contains more plagioclase and Gobabeb contains more olivine. Compact Reconnaissance Imaging Spectrometer for Mars (CRISM)-based estimates of mineralogy at the optical surface of Namib Dune and Mount Desert Island demonstrate that surface sands are enriched in olivine and depleted in plagioclase over Mount Desert Island relative to Namib Dune. Differences between CheMin-derived and CRISM-derived mineralogies suggest sorting by grain size on bedform to dune field scales. Crystal chemistry from CheMin suggests contributions from multiple igneous sources and the local bedrock.

Plain Language Summary Remote sensing data from orbit indicate that wind-blown sands in the Bagnold Dune Field in Gale crater, Mars, are sorted by their composition. The Mars Science Laboratory *Curiosity* rover studied the Bagnold Dune Field at two locations to investigate the chemical and mineral composition of the sands and why they are sorted across the dune field. Data from *Curiosity* show distinct differences between the minerals in the upwind portion of the dune field compared to the downwind portion, but these differences are not the same as those observed from orbit. The scale and location of the sampling by *Curiosity* compared to orbiters explains the discrepancy between the two techniques. Results from both techniques suggest subtle differences in mineralogy within a single dune and across the dune field that can be explained by sorting from wind and contribution from the erosion of local bedrock.

1. Introduction

After landing in Gale crater in August 2012, the Mars Science Laboratory *Curiosity* rover started its ascent toward Aeolis Mons (a.k.a., Mount Sharp) to characterize modern and ancient Martian environments. Along its traverse, *Curiosity* encountered an active eolian dune field, informally called the Bagnold Dune Field. Similar active, low-albedo dune fields and sand sheets are ubiquitous across Mars (Hayward et al., 2007), and orbiter-based thermal infrared and visible/shortwave-infrared (VSWIR) spectroscopic measurements of them are consistent with basaltic compositions (e.g., Bibring et al., 2005; Christensen et al., 2000; Poulet et al., 2009; Rogers & Bandfield, 2009; Stockstill-Cahill et al., 2008; Tirsch et al., 2011). The mineralogy within

the Bagnold Dune Field using orbital VSWIR observations from the Compact Reconnaissance Imaging Spectrometer for Mars (CRISM) demonstrates that basaltic minerals are segregated within the dune field. Barchanoidal dunes at the upwind margin and crests of linear dunes have stronger olivine signatures, whereas the linear dunes and the stoss sides of barchanoidal ridges have stronger high-Ca pyroxene signatures (Figure 1a; Lapotre, Ehlmann, Minson, Arvidson, et al., 2017; Seelos et al., 2014). Furthermore, olivine and plagioclase abundances are anticorrelated, and the apparent mineral segregation was thought to be related to wind sorting of minerals (e.g., by grain size, density, and shape) but also possibly by mixing of different sediment sources and/or a difference in dust cover (Lapotre, Ehlmann, Minson, Arvidson, et al., 2017). Possible sand source(s) include olivine-bearing units in Gale crater's walls (Buz et al., 2017; Ehlmann & Buz, 2015) and more local, perhaps more felsic materials possibly found in the crater walls or underlying the Bagnold Dune Field. *Curiosity* has investigated felsic targets in the conglomerates of the Aeolis Palus fan (Sautter et al., 2015), and the fluvio-lacustrine rocks that underlie the southwestern portion of the Bagnold Dune Field contain abundant plagioclase feldspar (Bristow et al., 2018).

Curiosity studied the Bagnold Dune Field during an extensive eolian science campaign consisting of two phases. Phase 1 was an examination of two barchan dunes along the northern, upwind margin of the dune field where the Gobabeb sample was scooped. Phase 2 examined linear dunes further south into the dune field where the Ogunquit Beach sample was scooped (Figure 1a; Bridges & Ehlmann, 2017; Lapotre & Rampe, 2018). Here we focus on addressing compositional variations across the Bagnold Dunes, using both rover and CRISM data, and on how ground and orbiter-based inferences can complement one another. We first report on the CheMin-derived mineralogy of sands sampled from the linear dunes during Phase 2 of the campaign and compare these results to the mineralogy of sands sampled from the dune field's upwind margin during Phase 1, which was previously described in depth by Achilles et al. (2017) and Ehlmann et al. (2017). We compare CheMin mineralogy to CRISM-derived mineralogy for undisturbed surfaces at the barchan and linear dunes closest to the CheMin sampling sites. Finally, we discuss how the two data sets can be used in a value-added manner to better understand sediment sorting and sources within Martian dune fields.

2. Data Collection and Processing

2.1. CheMin

CheMin is a charge-coupled device (CCD)-based transmission X-ray diffraction (XRD)/X-ray fluorescence instrument inside the body of the rover that employs Co radiation. The 2θ range is 2° to 52° with 0.3° angular resolution. Piezoelectric-induced vibrations create grain motion in cells with an active volume of 10 mm^3 (Blake et al., 2012). The two-dimensional CCD XRD patterns are converted to characteristic one-dimensional patterns with modified open-source GSE_ADA software (Dera et al., 2013). Cell offsets from the ideal diffraction position were determined by an internal calibration method based on refined unit cell parameters of plagioclase (Morrison, Downs, Blake, Prabhu, et al., 2018; Morrison, Downs, Blake, Vaniman, et al., 2018).

During the Bagnold Dunes campaign, two loose sand samples were scooped, sieved, and delivered to instruments inside the rover. These samples were collected from the surface to a few centimeters deep within the sands. Thus, the samples analyzed by CheMin are dominated by subsurface material. The Phase 1 Gobabeb sample was collected adjacent to the crest of a large ripple from the secondary slip face of the Namib barchan dune. The Phase 2 Ogunquit Beach sample was collected from the trough of a ripple in the Mount Desert Island ripple field (Figure 2a). Samples were processed by the rover's Sample Acquisition Sample Processing and Handling system and the Collection and Handling for In situ Martian Rock Analysis (CHIMRA) system (Anderson et al., 2012), and ~75 mm^3 of the $<$150-μm size fraction was delivered to CheMin Kapton cell 1A (Figure 2b).

Ogunquit Beach was scooped on sol 1650 but not delivered to CheMin until sol 1831 because of an anomaly in drill actuators. Three nights of analysis (a total of 22 hr of integration) were acquired on sols 1831, 1842, and 1847 by inducing piezoelectric vibrations on a neighboring cell pair (cell pair 0) to prevent sample ejection from the cell, as happened with the first analysis of a scooped sand (the Rocknest sample as described by Bish et al., 2013). Mineral abundances and unit cell parameters of major phases were quantified by Rietveld refinement of the 1-D patterns (e.g., Bish & Howard, 1988) using Materials Data Inc. Jade software. Abundances of X-ray amorphous materials and phyllosilicates were determined using a modified version

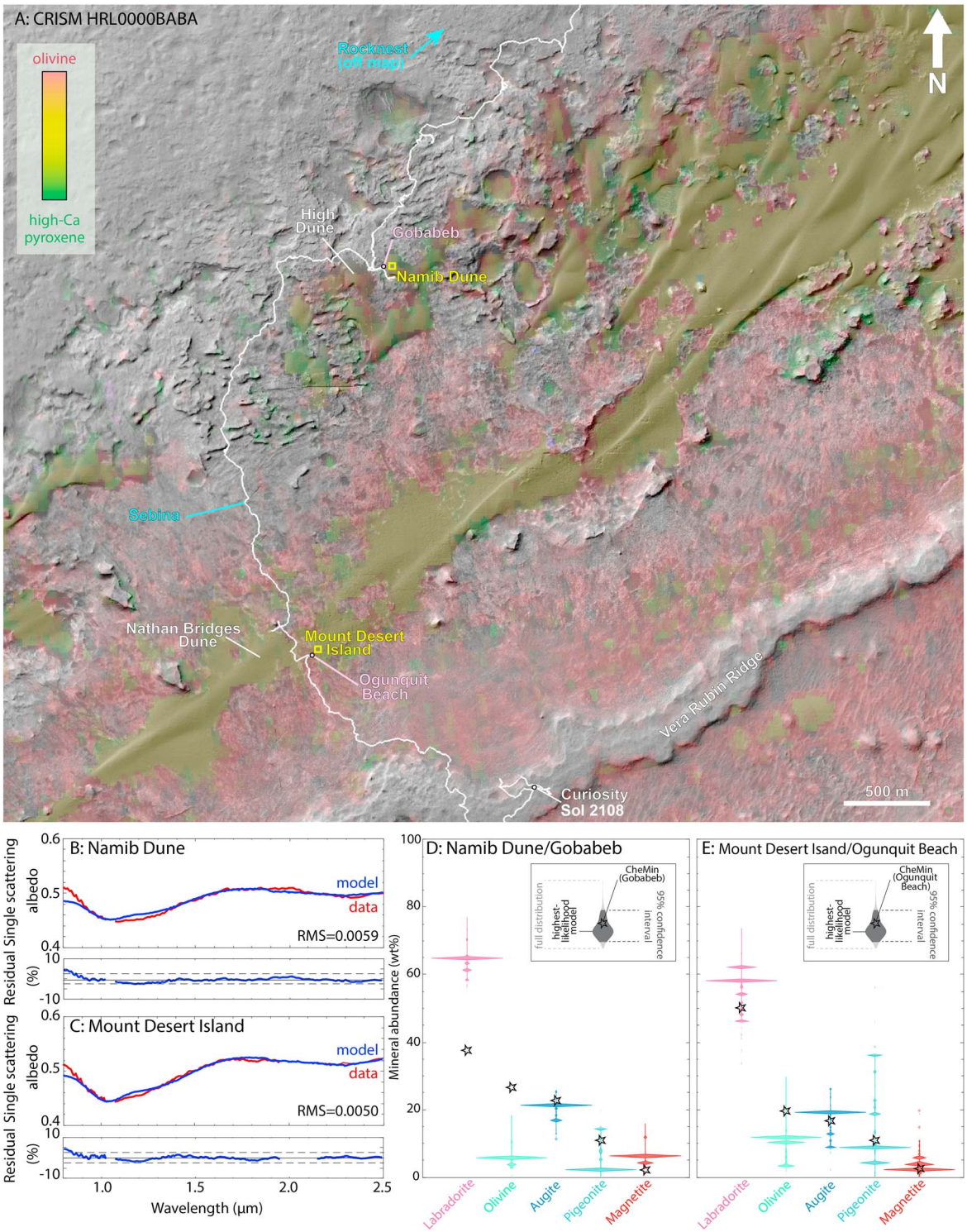

Figure 1. (a) Relative strength of olivine (OLINDEX3; red; range set to 0.024–0.075), high-calcium pyroxene (HCPINDEX2; green; range set to 0.0–0.0074), and low-calcium pyroxene (LCPINDEX2; blue; no values above 0.0 were found) signatures from CRISM parameter map data overlain onto a High Resolution Imaging Science Experiment-derived shaded relief map (Parker & Calef III, 2016). *Curiosity*'s traverse is outlined in white. Yellow rectangles show locations of the 3 × 3 CRISM pixels used for modeling; pink labels indicate CheMin samples within the dune field whereas light blue labels indicates other CheMin samples of interest. (b, c) Single scattering albedo spectra (red) and highest-likelihood modeled spectra (blue) for Namib Dune (b) and Mount Desert Island (c) along with their respective residuals (data/model). (d, e) CRISM-derived probability densities of abundances (wt.%) for each crystalline endmember phase (violins) and comparison with closest CheMin target (star) for Namib Dune (d) and Mount Desert Island (e). CheMin abundances were renormalized to only include crystalline phases used for CRISM modeling. CheMin = Chemistry and Mineralogy; CRISM = Compact Reconnaissance Imaging Spectrometer for Mars.

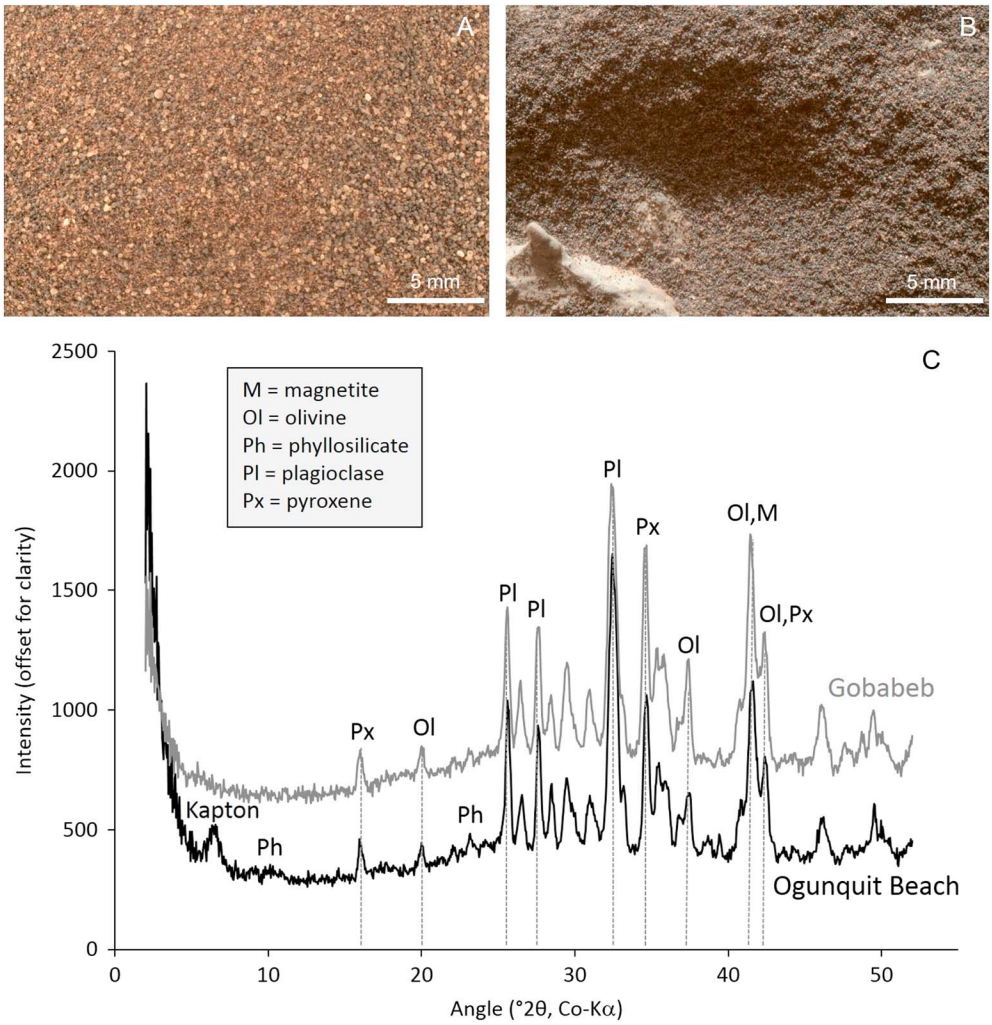

Figure 2. (a) Mars Hand Lens Imager focus merge product of Ogunquit Beach scooping location before sampling (target: Avery Peak, product 1651MH0007030000603240R00). (b) Mars Hand Lens Imager focus merge product of Ogunquit Beach <150-μm dump pile (product 1971MH0001630000504768R000). (c) Chemistry and Mineralogy X-ray diffraction patterns of Ogunquit Beach and Gobabeb from three nights of analysis.

of the full pattern fitting software FULLPAT (Chipera & Bish, 2002), which utilizes a library of XRD patterns of crystalline, poorly and paracrystalline, and X-ray amorphous materials. We also estimated the composition of the X-ray amorphous component from mass balance calculations using the abundance and composition of all crystalline phases identified in Rietveld refinements and the bulk chemistry of the <150-μm size fraction as measured by the Alpha Particle X-ray Spectrometer (APXS) of the post-sieve dump pile (e.g., Morrison, Downs, Blake, Vaniman, et al., 2018).

2.2. CRISM

CRISM is a VSWIR hyperspectral imager onboard the Mars Reconnaissance Orbiter and collecting radiance data from the Martian surface at 544 discrete wavelengths spanning the 0.4- to 4.0-μm wavelength range (Murchie et al., 2009). Targeted observations may be collected in several modes, each corresponding to different spatial resolutions: half-resolution short/long (HRS/HRL; 36 m per pixel), full-resolution targeted (FRT; ~18 m per pixel), and along-track oversampled (ATO; 18 m per pixel).

We processed five CRISM scenes covering the Bagnold Dunes (HRL0000BABA, FRT0000B6F1, FRT00021C92, FRT0001FD99, and ATO0002EC79), removing contributions from gases and aerosols, and retrieving single scattering albedos as discussed in Kreisch et al. (2017). Spectra retrieved for the Namib Dune and Mount

Desert Island sampling regions (Figure 1a) were found to be similar in shape for all scenes, although absolute amplitudes varied from scene to scene. These variations are a consequence of imperfect knowledge of dust and ice atmospheric opacities, of the single particle phase function assumed for surface scattering, and of the difficulties associated with retrieving data for exactly the same several pixels adjacent to *Curiosity*'s sand sampling sites from scene to scene. Of the five scenes, only HRL0000BABA and FRT0001FD99 cover both sand sampling sites, such that using data from those minimizes uncertainty associated with scene-to-scene variations. We illustrate the overall dune mineralogy using HRL0000BABA, with its 36-m-per-pixel resolution (Figure 1a), and also use data retrieved from this scene processed to 12 m per pixel to retrieve mean spectra for a 3×3 pixel area on the dunes adjacent to the sampling sites (Figures 1b and 1c). Our processing explicitly removes the spatial point spread function smearing from the data, minimizing the brightness spread of surrounding pixels into the dune-specific pixel areas. Spectra for FRT0001FD99 are compromised by relatively high inferred dust opacities (1.04 for FRT0001FD99 vs. 0.53 for HRL0000BABA), warm detector temperatures (-144 vs. -152 °C), the fact that the Namib Dune site is at the very edge of the scene, and a noticeable amplitude shading from the top to the bottom of the map-projected versions of FRT0001FD99.

Endmember phases used for spectral modeling were selected based on the presence of clear spectral signatures in single scattering albedo (SSA) data (e.g., olivine and pyroxenes) and expectations from geological context (e.g., plagioclase and magnetite; Lapotre, Ehlmann, Minson, Arvidson, et al., 2017). The final set of endmember phases included one olivine (Fo 51), two pyroxenes (augite and pigeonite), labradorite, magnetite, and basaltic glass to model the presence of an amorphous component (see Table S1 and Figure S1 for endmember spectra). The precise chemistry of solid solutions used for CRISM modeling was chosen on the basis of how they affected spectral fits—no a priori ground knowledge was used (Lapotre, Ehlmann, Minson, Arvidson, et al., 2017). Optical constants for these selected endmember phases were derived following the methodology described in Lapotre, Ehlmann, Minson, Arvidson, et al. (2017).

We then applied the Markov chain Monte Carlo algorithm of Lapotre, Ehlmann, & Minson (2017) for retrievals of mineral abundances and grain sizes from SSA data. Markov chains of 250,000 models were built for each spectrum, yielding full probability densities of mineral abundances and grain sizes permitted by the data at each location. Although we present the full inverted probability densities, we chose to illustrate inverted modal mineralogy by their corresponding highest marginal likelihood model (HMLM). Whereas the HMLM is not the overall best fit to the data, it uses the modal abundance from each endmember's posterior probability.

We emphasize that CRISM-retrieved mineralogy and grain sizes reflect those found within the typical skin depth penetrating into grains (e.g., Clark & Roush, 1984), which typically is ~1–10s μm, such that CRISM is sensing the very top surface of the dunes and integrates its composition over horizontally extensive, decameter-scale undisturbed areas. In contrast, CheMin analyzes samples with typical volumes of ~10s mm^3, scooped from a few centimeters below the surface and sieved to <150 μm. Furthermore, a single sample from a dune would not capture the compositional variations expected within an active dune, but CheMin data provide definitive quantitative mineralogy, an estimate on X-ray amorphous abundance, and crystal chemistry of major minerals. As a result, CRISM- and CheMin-derived mineralogies provide different but complementary information about spatial compositional variability within eolian sands.

3. Results

3.1. CheMin

Basaltic minerals and X-ray amorphous phases dominate the Ogunquit Beach sample (Table 1; Figure 2c). Major mineral phases identified from Rietveld refinements include (relative to the crystalline fraction) plagioclase feldspar (47.1 wt.%), olivine (18.2 wt.%), augite (15.7 wt.%), and pigeonite (10.2 wt.%). The crystal chemistry of these phases derived from unit cell parameters (Table S2) show the following mineral compositions: plagioclase $An_{48(5)}$, olivine $Fo_{60(3)}$, augite $(Mg_{1.27(19)}Ca_{0.66(7)}Fe_{0.08(23)})Si_2O_6$, and pigeonite $(Mg_{1.23(21)}Fe_{0.63(29)}Ca_{0.15(11)})Si_2O_6$ (Table 2). Values in parentheses represent 1σ errors for the final digits. Overlapping pyroxene peaks and the relatively low angular resolution of CheMin result in larger uncertainties in pyroxene compositions (e.g., Achilles et al., 2017). Minor phases include magnetite (2.5 wt.%), hematite (2.3 wt.%), and anhydrite (2.3 wt.%). Quartz (1.6 wt.%) is present near the detection limit of CheMin (Blake et al., 2012).

Table 1
Mineral and Amorphous Abundances for All Loose Sediment Samples Measured to Date by CheMin, and Highest-Likelihood Abundances as Estimated From CRISM

	Ogunquit Beach (linear)			Gobabeb (barchan)		Rocknest		Namib Dune (CRISM)	Mount Desert Island (CRISM)
	Crystalline[a]	Xtal +Amor[b]	No phyllo[c]	Crystalline	Xtal +Amor	Crystalline	Xtal +Amor		
Plagioclase	47.1(10)	24.7(5)	26.7(5)	36.5(8)	23.7(8)	40.7(5)	26.3(7)	33.80	43.05
Olivine	18.2(7)	9.6(3)	10.4(4)	25.8(4)	16.8(6)	20.5(4)	13.3(4)	3.05	8.80
Augite	15.7(18)	8.2(9)	8.9(10)	22.0(4)	14.3(6)	18.1(13)	11.7(9)	11.05	14.10
Pigeonite	10.2(6)	5.4(3)	5.8(3)	10.6(4)	6.9(6)	12.3(12)	8.0(8)	1.10	6.65
Magnetite	2.5(3)	1.3(2)	1.4(2)	2.1(2)	1.4(2)	2.5(5)	1.8(3)	3.10	1.60
Hematite	2.3(3)	1.2(2)	1.3(2)	0.9(1)[d]	0.6(2)	1.4(3)[d]	0.9(2)	N/A	N/A
Anhydrite	2.3(3)	1.2(2)	1.3(2)	1.3(1)[d]	0.8(1)	1.6(1)[d]	1.0(1)	N/A	N/A
Quartz	1.6(2)[d]	0.8(1)	0.9(1)	0.8(1)[d]	0.5(1)	1.3(3)[d]	0.8(2)	N/A	N/A
Ilmenite	—	—	—	—	—	1.3(5)	0.9(3)	N/A	N/A
Phyllosilicate	—	7.4(30)	—	——	—	—	—	N/A	N/A
Amorphous[e]	—	40(15)[f]	43(16)	—	35(15)[f]	—	35(15)	47.90	25.80

Note. Abundances are in weight percent and CheMin uncertainties in parentheses are 1σ. CRISM uncertainties are shown in Figure 1 for crystalline phases. CheMin = Chemistry and Mineralogy; CRISM = Compact Reconnaissance Imaging Spectrometer for Mars.
[a]Crystalline column includes mineral abundances renormalized to 100% crystalline phases (i.e., no amorphous or phyllosilicate components). [b]Xtal+Amor column includes mineral, amorphous, and phyllosilicate abundances. [c]No phyllo column includes mineral and amorphous abundances renormalized to 100% without phyllosilicate abundance. [d]At or below the CheMin detection limit. [e]Basaltic glass was used as an amorphous endmember for CRISM modeling. [f]Constrained by FULLPAT; Alpha Particle X-ray Spectrometer-constrained value is ~33% amorphous for Ogunquit Beach and ~42% amorphous for Gobabeb.

A weak peak in the pattern near 10° 2θ (Figure 2c) indicates the presence of ~7 wt.% phyllosilicate in Ogunquit Beach. However, phyllosilicates were neither detected from orbit nor identified in the Gobabeb sample with CheMin (Achilles et al., 2017). Mars Hand Lens Imager images of the CheMin funnel before and after delivery of Ogunquit Beach indicate that phyllosilicates in Ogunquit Beach likely resulted from contamination from the previously delivered phyllosilicate-rich sample Sebina (Bristow et al., 2018; Figure S2). The funnel image prior to delivery shows dark brown material near the center of the funnel, whereas the image after delivery shows a relative absence of this dark material, suggesting that the dark material was incorporated into the Ogunquit Beach sample. The absence of evidence for phyllosilicates in H_2O release data for the Ogunquit Beach sample measured by Sample Analysis at Mars instrument (Stern et al., 2018) further indicates that contamination from Sebina came from the CheMin funnel rather than CHIMRA. In Table 1, we renormalize mineral abundances in Ogunquit Beach to exclude the phyllosilicate contamination (see supporting information S1 for further information on contamination from Sebina [Bristow et al., 2018; Sposito et al., 1999; Stern et al., 2018; Sutter et al., 2017]).

Table 2
Crystal Chemistry of Major Minerals in Ogunquit Beach, Gobabeb, and Rocknest

Ogunquit Beach	
Plagioclase	$(Ca_{0.48(5)}Na_{0.52})(Al_{1.48}Si_{2.52})O_8$
Olivine	$(Mg_{1.19(6)}Fe_{0.81})SiO_4$
Augite	$(Mg_{1.27(19)}Ca_{0.66(7)}Fe_{0.08(23)})Si_2O_6$
Pigeonite	$(Mg_{1.23(21)}Fe_{0.63(29)}Ca_{0.15(11)})Si_2O_6$
Gobabeb[a]	
Plagioclase	$(Ca_{0.63(5)}Na_{0.37})(Al_{1.63}Si_{2.37})O_8$
Olivine	$(Mg_{1.08(3)}Fe_{0.92})SiO_4$
Augite	$(Mg_{0.89(8)}Ca_{0.73(3)}Fe_{0.38(9)})Si_2O_6$
Pigeonite	$(Mg_{0.95(12)}Fe_{0.99(17)}Ca_{0.06(8)})Si_2O_6$
Rocknest[a]	
Plagioclase	$(Ca_{0.49(4)}Na_{0.51})(Al_{1.49}Si_{2.51})O_8$
Olivine	$(Mg_{1.14(3)}Fe_{0.86})SiO_4$
Augite	$(Mg_{0.94(9)}Ca_{0.72(4)}Fe_{0.34(10)})Si_2O_6$
Pigeonite	$(Mg_{0.97(8)}Fe_{1.03(9)})Si_2O_6$

[a]From Achilles et al. (2017).

FULLPAT analyses suggest the presence of 40(15) wt.% X-ray amorphous materials, which are best fit by a combination of basaltic and rhyolitic glasses. The XRD patterns of X-ray amorphous phases with different compositions (e.g., amorphous silicates and sulfates; Morris et al., 2015), however, are similar and may substitute for one another in FULLPAT models. We estimated the composition of the X-ray amorphous component using the phyllosilicate-free mineral abundances from Rietveld refinements, crystal chemistry, amorphous abundance from FULLPAT, and the APXS-measured composition of the <150-μm dump pile (Table S4). Our calculations suggest the amorphous component is comprised of SiO_2 (~46 wt.%), FeO_T (~22 wt.%), Al_2O_3 (~7 wt.%), SO_3 (~6 wt.%), CaO (~5 wt.%), Na_2O and MgO (~3 wt.% each), TiO_2 and P_2O_5 (~2 wt.% each), and minor (<2 wt.% each) Cl, K_2O, Cr_2O_3, and MnO. The composition of the amorphous component also includes crystalline phases below the CheMin detection limit.

3.2. CRISM

By design, the endmember phases used for modeling yield low-root-mean-square fits ($<6 \times 10^{-3}$ and residuals typically <2.5%) to the data

at both locations. Figures 1b and 1c illustrate the goodness of spectral fits through the example of the HMLM models.

At both locations, significant amounts of basaltic glass (HMLM 25–50 wt.%) seem to be required by the data (Table 1). However, the difference in inverted glass abundances between both locations may result from first-order albedo/spectral slope matching because basaltic glass is relatively featureless in the VSWIR wavelength range (Figure S1). Furthermore, because a single phase function was used to derive SSA over the entire CRISM scene, the difference in inverted basaltic glass abundance at Namib Dune and Mount Desert Island may thus be an artifact of their separated locations within the CRISM scene.

When posterior probabilities are renormalized to crystalline phases only, both locations display similar mineralogy (Figures 1d and 1e), with dominant plagioclase (~60 wt.%), followed by pyroxenes (~25 wt.%), olivine (<~15 wt.%), and magnetite (<~5 wt.%). One important difference is that the augite composition derived from CheMin data of Ogunquit Beach may be very low in Fe whereas augite used in CRISM models contains Fe. More olivine and less plagioclase seem to be required by the data at Mount Desert Island than at Namib Dune, consistent with the trend observed by Lapotre, Ehlmann, Minson, Arvidson, et al. (2017) between barchan dunes and a linear dune further east. HMLM grain sizes yield weighted average effective sizes in the coarse sand range (Table S3).

4. Discussion

The CheMin mineralogies of Gobabeb and Ogunquit Beach are broadly similar—both samples are dominated by plagioclase, olivine, augite, pigeonite, and X-ray amorphous materials and minor magnetite, hematite, anhydrite, and quartz. Distinct differences between the two samples are observed; Ogunquit Beach has more plagioclase than Gobabeb, whereas Gobabeb has more olivine than Ogunquit Beach (Table 1), consistent with enrichment in mafic phases found at ripple crests in active ripples by APXS (e.g., O'Connell-Cooper et al., 2017, 2018). The crystal chemistry of the major phases from CheMin suggests multiple igneous sources for all eolian samples measured to date. As was reported for Rocknest and Gobabeb (Achilles et al., 2017), olivine and pigeonite have similar molar Mg/(Mg + Fe) ratios, whereas augite is more magnesian, indicating augite and pigeonite are not in equilibrium with one another. This, in addition to the differences in An# between the samples (Table 2), suggests at least two basaltic igneous sources for the Bagnold Dunes.

Likewise the CRISM-derived mineralogies at Namib Dune and Mount Desert Island are broadly similar (Figures 1d and 1e), and differences between olivine and plagioclase abundances may largely be explained through their respective positions within the dune field. Segregation between felsic and mafic grains in eolian dune fields may occur through the effects of grain size and mineralogy (which in turn may affect grain density, grain shape, etc.) and has been observed on Earth and Mars (e.g., Chen et al., 2018; Lapotre, Ehlmann, Minson, Arvidson, et al., 2017; Mangold et al., 2011; Stockstill-Cahill et al., 2008). Dune fields in Iceland and the Badain Jaran Desert in China show a concentration of fine mafic grains downwind and a concentration of coarse felsic grains along the fields' trailing edges, demonstrating that particle weight controls variations in mineral composition across a dune field. Particle shape may also play a significant role in mineral segregation, where rounded grains and euhedral crystals favor migration, and flat grains (e.g., plagioclase) are not as easily transported (Mangold et al., 2011). However, we do not observe discrete elongated plagioclase crystals in Mars Hand Lens Imager images of the sand, such that plagioclase may instead be present in subangular lithic fragments, and feedbacks between particle weight and topography likely control the observed spatial variability over the Bagnold Dunes. Finer grains (mafic and felsic) may move up the stoss slopes of barchan dunes along the field's trailing edge, whereas the coarsest grains may be left as lags at the base of those dunes (e.g., Lapotre & Rampe, 2018; Weitz et al., 2018), consistent with strong CRISM olivine signatures there (Figure 1a). The grain size fraction that is readily transported across the dune field may then gradually get enriched in finer mafic grains with transport distance, explaining the CRISM-derived increase in olivine-to-plagioclase ratio between Namib Dune and Mount Desert Island.

Unsurprisingly, differences exist between CRISM- and CheMin-derived compositions (Figures 1d and 1e). CRISM- and CheMin-derived mineralogies are more similar at Mount Desert Island/Ogunquit Beach than at Namib Dune/Gobabeb. These differences can be directly related to both sample size and sample

location for each technique. At Gobabeb, CheMin sampled a ripple crest, which, while locally enriched in olivine, may not be representative of the dune-surface average composition. In contrast, CheMin sampled a ripple trough at Ogunquit Beach, which is expected to be more similar to average-surface composition as derived from CRISM. Furthermore, whereas the qualitative strengths of olivine and pyroxene signatures vary across the dune field (Figure 1a; Lapotre, Ehlmann, Minson, Arvidson, et al., 2017; Seelos et al., 2014), we did not observe changes in the olivine-to-pyroxene ratios in the CheMin data within the 1σ errors of our refinements (Table 1). However, the CheMin analysis was restricted to the <150-μm size fraction and may not have captured differences in abundances of the coarsest fraction. Furthermore, quantitative CRISM-based estimates actually yield a higher olivine-to-pyroxene ratio at Mount Desert Island than at Namib Dune, such that the qualitative trends observed in parameter maps may instead reflect trends in grain size or the effect of relatively featureless phases with broad and often shallow absorption features (e.g., plagioclase or glass) on those parameters (Lapotre, Ehlmann, Minson, Arvidson, et al., 2017). Alternatively, if the augite in Mount Desert Island has low Fe content, as suggested by crystal chemistry derived from CheMin, then this phase would not be easily detected by CRISM. Altogether, CheMin- and CRISM-derived mineralogies can be used to constructively constrain patterns and magnitude of wind sorting over the dune field in a complementary fashion.

In addition to wind sorting, spatial variations in composition may also point toward contribution from different local sediment sources. From CheMin, the refined compositions of olivine and pigeonite in Ogunquit Beach are within or very close to the 1σ error of those for Gobabeb, suggesting a similar sediment source for these minerals (Table 2). The differences in plagioclase and augite compositions between the two samples, however, are outside of the 1σ uncertainty (i.e., $An_{48(5)}$ and $Mg_{1.27(19)}Ca_{0.66(7)}Fe_{0.08(23)}$ for Ogunquit Beach and $An_{63(5)}$ and $Mg_{0.89(8)}Ca_{0.73(3)}Fe_{0.38(9)}$ for Gobabeb). The more sodic plagioclase in Ogunquit Beach could result from a different basaltic igneous source or from contribution of grains from the underlying Murray formation because plagioclase in samples measured from the Murray formation near Ogunquit Beach are ~$An_{40(6)}$ (Achilles, 2018). This difference in plagioclase composition may also result from contamination from Sebina. It is important to note that the plagioclase composition of the Rocknest sample ($An_{49(4)}$), scooped from an inactive sand patch near the landing site, is the same within error of the plagioclase composition in Ogunquit Beach (Table 2). The difference between the plagioclase in Rocknest and Gobabeb suggests that there is true variation in plagioclase composition in loose sediments in Gale crater, which may result from variable sediment sources.

Differences in the X-ray amorphous component compositions in Ogunquit Beach and Gobabeb may also be a result of different local sediment sources. The estimated compositions of the X-ray amorphous components of Ogunquit Beach and Gobabeb are broadly similar and are both dominated by SiO_2, FeO_T, Al_2O_3, and SO_3 (Tables S4 and S5). The compositions of the amorphous components in both samples are inconsistent with pure basaltic glass and could be comprised of a combination of volcanic and/or impact glass(es), weathered silicates, sulfates, and nanophase Fe-oxides (Achilles et al., 2017; Ehlmann et al., 2017). Ogunquit Beach has more FeO_T, MgO, and CaO, whereas Gobabeb has more SiO_2, Na_2O, and SO_3. Some of the bedrock near Gobabeb contains amorphous silica (Morris et al., 2016; Yen et al., 2017), whereas the local bedrock near Ogunquit Beach is relatively enriched in nanophase Fe oxides (Achilles, 2018), which could explain enrichments in FeO_T and SiO_2 in Ogunquit Beach and Gobabeb, respectively. Martian dust, which is enriched in nanophase Fe oxides (e.g., Morris et al., 2006), is an unlikely source of the Fe enrichment because active sediment transport was observed during Phase 2 (Baker et al., 2018).

Comparing the mineralogy of modern sands in Gale crater to ancient eolian sandstone from the Stimson formation may suggest different sediment sources for the eolian dune fields in the crater floor over time. Modern eolian samples have abundant olivine, pigeonite, and augite (i.e., high-Ca pyroxene), whereas samples from the Stimson eolian sandstone lack olivine and contain abundant pigeonite and orthopyroxene (i.e., low-Ca pyroxene [Yen et al., 2017]). It is likely that the Stimson once contained olivine that has since been altered (Yen et al., 2017), but the presence of augite in modern sediments and orthopyroxene in ancient sandstone may point toward shifts in sediment source over time. One important caveat is that overlapping XRD peaks from different pyroxenes result in relatively large errors in abundances and refined crystal chemistry. More samples from future eolian sandstones as *Curiosity* climbs Mount Sharp would help further investigate changes in sediment source spatially and through time.

Acknowledgments
We gratefully acknowledge support from the NASA Mars Science Laboratory Mission and the MSL engineering and science teams for executing the Bagnold Dunes campaign. We thank Kevin Cannon and Kim Seelos for their thoughtful reviews of this manuscript. Mission data (i.e., collected by CheMin, APXS, and CRISM) supporting the conclusions can be obtained from the Planetary Data System Geosciences Node. Additional data supporting the conclusions are found in the supporting information. This manuscript is dedicated to Nathan Bridges, who helped design this campaign and whose passion and enthusiasm are dearly missed.

References

Achilles, C. N. (2018). Analyses of crystalline and X-ray amorphous materials in Gale crater rocks and soils. (Doctoral dissertation). University of Arizona Open Repository.

Achilles, C. N., Downs, R. T., Ming, D. W., Rampe, E. B., Morris, R. V., Treiman, A. H., et al. (2017). Mineralogy of an active eolian sediment from the Namib dune, Gale crater, Mars. *Journal of Geophysical Research: Planets*, *122*, 2344–2361. https://doi.org/10.1002/2017JE005262

Anderson, R. C., Jandura, L., Okon, A. B., Sunshine, D., Roumeliotis, C., Beegle, L. W., et al. (2012). Collecting samples in Gale Crater, Mars: An overview of the Mars Science Laboratory sample acquisition, sample processing and handling system. *Space Science Reviews*, *170*(1-4), 57–75. https://doi.org/10.1007/s11214-012-9898-9

Baker, M., Lapotre, M. G. A., Bridges, N. T., Minitti, M. E., Newman, C. E., Ehlmann, B. L., et al. (2018). The Bagnold Dunes in southern summer: Active sediment transport on Mars observed by the Curiosity rover. *Geophysical Research Letters*, *45*. https://doi.org/10.1029/2018GL079040

Bibring, J. P., Langevin, Y., Gendrin, A., Gondet, B., Poulet, F., Berthé, M., et al. (2005). Mars surface diversity as revealed by the OMEGA/Mars Express observations. *Science*, *307*(5715), 1576–1581. https://doi.org/10.1126/science.1108806

Bish, D. L., Blake, D. F., Vaniman, D. T., Chipera, S. J., Morris, R. V., Ming, D. W., et al. (2013). X-ray diffraction results from Mars Science Laboratory: Mineralogy of Rocknest at Gale crater. *Science*, *341*(6153). https://doi.org/10.1126/science.1238932

Bish, D. L., & Howard, S. A. (1988). Quantitative phase analysis using the Rietveld method. *Journal of Applied Crystallography*, *21*(2), 86–91. https://doi.org/10.1107/s0021889887009415

Blake, D. F., et al. (2012). Characterization and calibration of the CheMin mineralogical instrument on Mars Science Laboratory. *Space Science Reviews*, *170*(1-4), 341–399. https://doi.org/10.1007/s11214-012-9905-1

Bridges, N. T., & Ehlmann, B. L. (2017). The Mars Science Laboratory (MSL) Bagnold Dunes Campaign Phase I: Overview and introduction to the special issue. *Journal of Geophysical Research: Planets*, *123*, 3–19. https://doi.org/10.1002/2017JE005401

Bristow, T. F., Rampe, E. B., Achilles, C. N., Blake, D. F., Chipera, S. J., Craig, P., et al. (2018). Clay mineral diversity and abundance in sedimentary rocks of Gale crater, Mars. *Science Advances*, *4*(6), eaar3330. https://doi.org/10.1126/sciadv.aar3330

Buz, J., Ehlmann, B. L., Pan, L., & Grotzinger, J. P. (2017). Mineralogy and stratigraphy of the Gale crater rim, wall, and floor units. *Journal of Geophysical Research: Planets*, *122*, 1090–1118. https://doi.org/10.1002/2016JE005163

Chen, Q., Li, Z., Dong, S., Wang, N.'., Lai, D. Y. F., & Ning, K. (2018). Spatial variations in the chemical composition of eolian sediments in hyperarid regions: A case study from the Badain Jaran Desert, northwestern China. *Journal of Sedimentary Research*, *88*, 290–300. https://doi.org/10.2110/jsr.2018.11

Chipera, S. J., & Bish, D. L. (2002). FULLPAT: A full-pattern quantitative analysis program for X-ray powder diffraction using measured and calculated patterns. *Journal of Applied Crystallography*, *35*(6), 744–749. https://doi.org/10.1107/S0021889802017405

Christensen, P. R., Bandfield, J. L., Smith, M. D., Hamilton, V. E., & Clark, R. N. (2000). Identification of a basaltic component on the Martian surface from thermal emission spectrometer data. *Journal of Geophysical Research*, *105*(E4), 9609–9621. https://doi.org/10.1002/1999JE001127

Clark, R. N., & Roush, T. L. (1984). Reflectance spectroscopy: Quantitative analysis techniques for remote sensing applications. *Journal of Geophysical Research*, *89*(B7), 6329–6340. https://doi.org/10.1029/JB089iB07p06329

Clark, R. N., Swayze, G. A., Wise, R., Livo, K. E., Hoefen, T. M., Kokaly, R. F., et al. (2007). USGS Digital Spectral Library splib06a, edited, US Geological Survey Reston, VA.

Dera, P., Zhuravlev, K., Prakapenka, V., Rivers, M. L., Finkelstein, G. J., Grubor-Urosevic, O., et al. (2013). High pressure single-crystal micro X-ray diffraction analysis with GSE_ADA/RSV software. *High Pressure Research*, *33*(3), 466–484. https://doi.org/10.1080/08957959.2013.806504

Ehlmann, B. L., & Buz, J. (2015). Mineralogy and fluvial history of the watersheds of Gale, Knobel, and Sharp craters: A regional context for the Mars Science Laboratory Curiosity's exploration. *Geophysical Research Letters*, *42*, 264–273. https://doi.org/10.1002/2014GL062553

Ehlmann, B. L., Edgett, K. S., Sutter, B., Achilles, C. N., Litvak, M. L., Lapotre, M. G. A., et al. (2017). Chemistry, mineralogy, and grain properties at Namib and High dunes, Bagnold dune field, Gale crater, Mars: A synthesis of Curiosity rover observations. *Journal of Geophysical Research: Planets*, *122*, 2510–2543. https://doi.org/10.1002/2017JE005267

Hayward, R. K., Mullins, K. F., Fenton, L. K., Hare, T. M., Titus, T. N., Bourke, M. C., et al. (2007). Mars global digital dune database and initial science results. *Journal of Geophysical Research*, *112*, E11007. https://doi.org/10.1029/2007JE002943

Kreisch, C. D., O'Sullivan, J. A., Arvidson, R. E., Politte, D. V., He, L., Stein, N. T., et al. (2017). Regularization of Mars Reconnaissance Orbiter CRISM along-track oversampled hyperspectral imaging observations of Mars. *Icarus*, *282*, 136–151. https://doi.org/10.1016/j.icarus.2016.09.033

Lapotre, M. A., & Rampe, E. B. (2018). Curiosity's investigation of the Bagnold Dunes, Gale crater: Overview of the two-phase scientific campaign and introduction to the special collection. *Geophysical Research Letters*, *45*. https://doi.org/10.1029/2018GL079032

Lapotre, M. G. A., Ehlmann, B. L., & Minson, S. E. (2017). A probabilistic approach to remote compositional analysis of planetary surfaces. *Journal of Geophysical Research: Planets*, *122*, 983–1009. https://doi.org/10.1002/2016JE005248

Lapotre, M. G. A., Ehlmann, B. L., Minson, S. E., Arvidson, R. E., Ayoub, F., Fraeman, A. A., et al. (2017). Compositional variations in sands of the Bagnold Dunes, Gale Crater, Mars, from visible-shortwave infrared spectroscopy and comparison with ground truth from the Curiosity Rover. *Journal of Geophysical Research: Planets*, *122*, 2489–2509. https://doi.org/10.1002/2016JE005133

Mangold, N., Baratoux, D., Arnalds, O., Bardintzeff, J. M., Platevoet, B., Grégoire, M., & Pinet, P. (2011). Segregation of olivine grains in volcanic sands in Iceland and implications for Mars. *Earth and Planetary Science Letters*, *310*(3-4), 233–243. https://doi.org/10.1016/j.epsl.2011.07.025

Morris, R. V., , Rampe, E. B., Graff, T. G., Archer, P. D., Jr., Le, L., Ming, D. W., et al. (2015). Transmission X-ray diffraction (XRD) patterns relevant to the MSL CheMin amorphous component: Sulfates and silicates, *LPSC XLVI* Abstract 2434.

Morris, R. V., Vaniman, D. T., Blake, D. F., Gellert, R., Chipera, S. J., Rampe, E. B., et al. (2016). Silicic volcanism on Mars evidenced by tridymite in high-SiO_2 sedimentary rock at Gale crater. *Proceedings of the National Academy of Sciences of the United States of America*, *113*(26), 7071–7076. https://doi.org/10.1073/pnas.1607098113

Morris, R. V., et al. (2006). Mössbauer mineralogy of rock, soil, and dust at Gusev crater, Mars: Spirit's journey through weakly altered olivine basalt on the plains and pervasively altered olivine basalt in the Columbia Hills. *Journal of Geophysical Research*, *111*, E02S13. https://doi.org/10.1029/2005JE002584

Morrison, S. M., Downs, R. T., Blake, D. F., Prabhu, A., Eleish, A., Vaniman, D. T., et al. (2018). Relationships between unit-cell parameters and composition for rock-forming minerals on Earth, Mars, and other extraterrestrial bodies. *American Mineralogist*, *103*(6), 848–856. https://doi.org/10.2138/am-2018-6123

Morrison, S. M., Downs, R. T., Blake, D. F., Vaniman, D. T., Ming, D. W., Hazen, R. M., et al. (2018). Crystal chemistry of martian minerals from Bradbury Landing through Naukluft Plateau, Gale crater, Mars. *American Mineralogist*, *103*(6), 857–871. https://doi.org/10.2138/am-2018-6124

Murchie, S. L., Mustard, J. F., Ehlmann, B. L., Milliken, R. E., Bishop, J. L., McKeown, N. K., et al. (2009). A synthesis of Martian aqueous mineralogy after 1 Mars year of observations from the Mars Reconnaissance Orbiter. *Journal of Geophysical Research*, *114*, E00D06. https://doi.org/10.1029/2009JE003342

O'Connell-Cooper, C., Spray, J. G., Thompson, L. M., Gellert, R., Berger, J. A., Boyd, N. I., et al. (2018). APXS-derived chemistry across the Bagnold dune field. *Geophysical Research Letters*, *45*. https://doi.org/10.1029/2018GL079026

O'Connell-Cooper, C. D., Spray, J. G., Thompson, L. M., Gellert, R., Berger, J. A., Boyd, N. I., et al. (2017). APXS-derived chemistry of the Bagnold dune sands: Comparisons with Gale Crater soils and the global Martian average. *Journal of Geophysical Research: Planets*, *122*, 2623–2643. https://doi.org/10.1002/2017JE005268

Parker, T. and Calef III, F.J. (2016). MSL Gale Merged Digital Elevation Model, Publisher: PDS Annex, U.S. Geological Survey, URL: http://bit.ly/MSL_DEM.

Poulet, F., Bibring, J. P., Langevin, Y., Mustard, J. F., Mangold, N., Vincendon, M., et al. (2009). Quantitative compositional analysis of martian mafic regions using the MEx/OMEGA reflectance data 1. Methodology, uncertainties and examples of application. *Icarus*, *201*(1), 69–83. https://doi.org/10.1016/j.icarus.2008.12.025

Rogers, A. D., & Bandfield, J. L. (2009). Mineralogical characterization of Mars Science Laboratory candidate landing sites from THEMIS and TES data. *Icarus*, *203*(2), 437–453. https://doi.org/10.1016/j.icarus.2009.04.020

Seelos, K. D., Seelos, F. P., Viviano-Beck, C. E., Murchie, S. L., Arvidson, R. E., Ehlmann, B. L., & Fraeman, A. A. (2014). Mineralogy of the MSL Curiosity landing site in Gale crater as observed by MRO/CRISM. *Geophysical Research Letters*, *41*, 4880–4887. https://doi.org/10.1002/2014GL060310

Sposito, G., Skipper, N. T., Sutton, R., Park, S. H., Soper, A. K., & Greathouse, J. A. (1999). Surface geochemistry of the clay minerals. *Proceedings of the National Academy of Sciences of the United States of America*, *96*(7), 3358–3364. https://doi.org/10.1073/pnas.96.7.3358

Stern, J. C., Sutter, B., Douglas Archer, P., Eigenbrode, J. L., McAdam, A. C., Franz, H. B., et al. (2018). Major volatiles evolved from eolian materials in Gale Crater. *Geophysical Research Letters*, *45*. https://doi.org/10.1029/2018GL079059

Stockstill-Cahill, K. R., Anderson, F. S., & Hamilton, V. E. (2008). A study of low-albedo deposits within Amazonis Planitia craters: Evidence for locally derived ultramafic to mafic materials. *Journal of Geophysical Research*, *113*, E07008. https://doi.org/10.1029/2007JE003036

Sutter, B., McAdam, A. C., Mahaffy, P. R., Ming, D. W., Edgett, K. S., Rampe, E. B., et al. (2017). Evolved gas analyses of sedimentary rocks and eolian sediment in Gale Crater, Mars: Results of the Curiosity rover's sample analysis at Mars instrument from Yellowknife Bay to the Namib Dune. *Journal of Geophysical Research: Planets*, *122*, 2574–2609. https://doi.org/10.1002/2016JE005225

Tirsch, D., Jaumann, R., Pacifici, A., & Poulet, F. (2011). Dark aeolian sediments in Martian craters: Composition and sources. *Journal of Geophysical Research: Planets*, *116*, E03002. https://doi.org/10.1029/2009JE003562

Weitz, C., Sullivan, R. J., Lapotre, M. G. A., Rowland, S. K., Grant, J. A., Baker, M., & Yingst, R. A. (2018). Sand grain sizes and shapes in eolian bedforms at Gale crater, Mars. *Geophysical Research Letters*, *45*. https://doi.org/10.1029/2018GL078972

Yen, A. S., Ming, D. W., Vaniman, D. T., Gellert, R., Blake, D. F., Morris, R. V., et al. (2017). Multiple stages of aqueous alteration along fractures in mudstone and sandstone strata in Hale Crater, Mars. *Earth and Planetary Science Letters*, *471*, 186–198. https://doi.org/10.1016/j.epsl.2017.04.033